Research Article Vol. 58, No. 22 / 1 August 2019 / Applied Optics 6007

Noise-like mode-locked Yb-doped fiber laser in a linear cavity based on SnS_2 nanosheets as a saturable absorber

Jinjuan Gao,[1] Yong Zhou,[1] Yanjun Liu,[2] Xile Han,[1] Quanxin Guo,[1] Zhengyi Lu,[1] Linguang Guo,[1] Xinxin Shang,[1] Wenqing Yang,[1] Kangdi Niu,[1] Na Ming,[1] Zhihao Wang,[1] Huanian Zhang,[1,*] and Shouzhen Jiang[1,3]

[1]Shandong Provincial Key Laboratory of Optics and Photonic Device, School of Physics and Electronics, Shandong Normal University, Jinan 250014, China
[2]Department of Electrical and Electronic Engineering, Southern University of Science and Technology, Shenzhen 518055, China
[3]e-mail: jiang_sz@126.com
*Corresponding author: huanian_zhang@163.com

Received 11 April 2019; revised 10 June 2019; accepted 24 June 2019; posted 26 June 2019 (Doc. ID 364872); published 25 July 2019

In this study, a high-energy noise-like mode-locked Yb-doped fiber laser in a linear cavity was achieved with SnS_2-polyvinyl alcohol film as the saturable absorber. In addition, the nonlinear saturable absorption characteristics of the SnS_2 were investigated experimentally. The saturation intensity and modulation depth were about 6.01 MW/cm^2 and 8.68%, respectively. Under pump power of 422 mW, stable noise-like mode-locked operation with a maximum output power and largest single pulse energy of 9.50 mW and 18.1 nJ, respectively, was obtained. To the best of our knowledge, this study is the first to observe and experimentally investigate noise-like operation in a linear laser cavity. Our study may provide some valuable design guidelines for noise-like operation and create new directions for advanced photonic devices based on SnS_2. © 2019 Optical Society of America

https://doi.org/10.1364/AO.58.006007

1. INTRODUCTION

Mode-locked fiber lasers have aroused considerable attention for wide applications in the fields of practical industries, scientific research, etc. In addition, numerous nonlinear phenomena have been produced by mode-locked fiber lasers, e.g., conventional soliton mode-locked [1], all-normal dispersion [2], multiple-wavelength mode-locked [3], dissipative solitons [4], and noise-like mode-locked operation [5]. Noise-like mode-locked operation has the advantages of high energy, wide optical bandwidth, and short coherence. Liu *et al.* experimentally verified the formation of a noise-like square-wave pulse in a passively mode-locked erbium-doped fiber laser with large anomalous dispersion [6]. Moreover, a passively mode-locked soliton fiber ring laser with a dispersion managed cavity was reported [7]. However, these were all achieved in ring cavities. We first achieved a high-energy noise-like mode-locked Yb-doped fiber laser in a linear cavity using the tin disulfide (SnS_2)-polyvinyl alcohol (PVA) film as the saturable absorber (SA).

It is widely known that a nonlinear SA is an indispensable device of a mode-locked laser [8]. The most commonly used mode-locked fiber lasers are based on commercial semiconductor saturable absorber mirrors (SESAMs) [9,10]. However, SESAMs have a large cost and exhibit a narrow operation bandwidth (typically a few tens of nanometers [11]). Recently, two-dimensional (2D) materials have widely served as SAs for demonstrating passively Q-switched or mode-locked fiber lasers. For instance, carbon nanotubes (CNTs) are easy to prepare and cost less [12], whereas their absorption efficiency and bandwidth are related to diameter, which limits their application. Accordingly, it is urgent to find a SA that has a wide absorption range and ultra-fast recovery time. The appearance of graphene has overcome the weakness of CNTs. A graphene-based erbium-doped mode-locked fiber laser was initially reported in 2010 [13], with the advantages of wide absorption range, easy preparation, low cost, fast recovery time, high damage threshold, and low saturation threshold. However, the zero-bandgap structure limits its applications for optoelectronic devices. A topological insulator (TI) has been confirmed to exhibit unique photonics properties owing to its broadband spectral response ranging from terahertz to infrared, which was due to its intrinsic gapless surface band [14]. In particular, transition metal dichalcogenides (TMDs), specifically molybdenum disulfide (MoS_2), molybdenum diselenide (MoS_2), tungsten disulfide (WS_2), tungsten diselenide (WSe_2), and tin selenide ($SnSe_2$) [15–24], have shown their significant feasibility in the sphere of nonlinear optics and photo-electronics because of their properties of high three-order optical nonlinear susceptibility, ultra-fast carrier dynamics, and semi-conductive capabilities with a tunable bandgap [25]. Moreover, ReS_2 served

as a SA, and self-started mode-locking operation in an Er-doped fiber laser was reported by Cui *et al.* in 2017 [26]. Furthermore, film-type ReS_2-PVA-based harmonic mode-locking operation in an erbium-doped fiber laser was also reported [27].

Compared to the mentioned TMDs, SnS_2 has aroused more attention because it is low cost, is easily prepared, has a suitable bandgap, is environmentally friendly, and is earth abundant. In addition, SnS_2 is an *n*-type direct bandgap semiconductor with a value of 2.24 eV; it has a CdI_2 crystal structure with a sandwich structure, composed of two layers of close-packed sulfur anions and one layer of tin cations [28–31]. SnS_2 nanosheets have shown excellent performance as SAs for passively *Q*-switched and mode-locked Er-doped fiber lasers with ring cavities [25,32]. However, for conventional soliton mode-locked fiber lasers in a ring cavity, the output power and single pulse power of a mode-locked fiber laser usually have low values. Zhang *et al.* generated large energy pulse with single pulse energy of 7.3 nJ [33] in an erbium-doped fiber laser passively mode locked with atomic layer graphene. Li *et al.* achieved high-energy mode-locking operation in an all-normal-dispersion Yb-doped mode-locked fiber laser based on a Bi_2Te_3 topological insulator, obtaining a maximum single pulse energy of 2 nJ [34]. Thus far, SnS_2 nanosheets as SAs have not achieved high-energy mode-locking operation in linear or ring cavities. Thus, we conducted a new attempt in a linear cavity and found some different phenomena.

In this paper, SnS_2 nanosheets were prepared and first used as SA in a linear cavity to demonstrate a noise-like mode-locked Yb-doped fiber laser with high-energy mode-locking operation. The maximum output power and highest single pulse energy were 9.50 mW and 18.1 nJ, respectively. When the pump power increased from 60 to 422 mW, the pulse width increased from 0.18 to 0.36 μs with a pulse repetition rate of 526 kHz. In addition, we have demonstrated a noise-like mode-locked Yb-doped fiber laser in a linear cavity operated at a central wavelength of 1065.24 nm with a 3 dB bandwidth of 0.022 nm. Our experimental results show that SnS_2 has significant potential in obtaining a high-energy noise-like mode-locking operation in a linear cavity.

2. PREPARATION AND CHARACTERIZATION OF MATERIALS

In this experiment, the preparation process of the SA is described as follows. First, an SnS_2 dispersion solution was produced by adding 1 g SnS_2 nanosheets into 100 ml alcohol (30%). Subsequently, the mixture was placed in the ultrasonic cleaner for 12 h. Second, the SnS_2 dispersion and 5 wt.% PVA solution were mixed at a volume ratio of 2:3. The resulting dispersion was placed in an ultrasonic cleaner for 4 h to produce the SnS_2-PVA dispersion solution. Third, 150 μl SnS_2-PVA dispersion solution was spin-coated on a glass substrate and then incubated in an oven for 48 h at 30°C. Next, a thin SnS_2-PVA film was prepared. Finally, a 1 mm × 1 mm thin film was cut off and put on the end face of the photonic crystal (PC) fiber head as SAs.

To analyze the structure of the SnS_2 nanosheets, the following characterization was achieved. In Fig. 1(a), a scanning electron microscope (SEM) image under a resolution of 1 μm shows that SnS_2 nanosheets exhibit a layered structure.

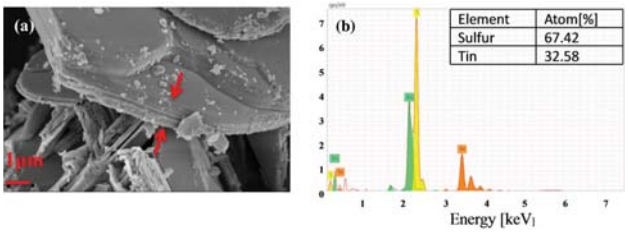

Fig. 1. (a) SEM image of the SnS_2 nanosheets. (b) EDX spectroscopy of the SnS_2 nanosheets. Inset: the atomic ratio of sulfur and tin.

Energy dispersion x-ray (EDX) was used to analyze the element component of the SnS_2 nanosheets. Figure 1(b) suggests that the corresponding peaks are clearly associated with sulfur and tin. To observe the sample more clearly, the SnS_2 nanosheets received the "gold plating" process. Accordingly, the peaks of Au are shown in Fig. 1(b) as well. As shown in the inset of Fig. 1(b), the atomic ratio of sulfur and tin is about 2:1.

To characterize the layered structure properties of the SnS_2, a JEM-2100 microscope with an optical resolution of 100 nm was employed to take a transmission electron microscope (TEM) image of the SnS_2 nanosheet dispersion solution. Figure 2(a) suggests the SnS_2 is obviously layered. The TEM image of the SnS_2 implies that the SnS_2 prepared here is layered with a high crystallinity. The SnS_2 dispersion solution is shown in the inset of Fig. 2(a). Next the high-quality structure was evidenced by the HRTEM image in Fig. 2(b), where regular diffraction fringes with a resolution of 5 nm can be clearly observed.

Subsequently, the crystal structure of the SnS_2 nanosheets was further analyzed using x-ray diffraction (XRD) technology. Figure 3(a) shows the obviously high diffraction peaks at the (001) plane in the XRD pattern, suggesting that the SnS_2 nanosheets prepared here are well-layered. Figure 3(b) gives the Raman spectrum of the layered SnS_2. Two Raman shift peaks corresponding to the A_{1g} and E_g symmetry intralayer modes at 313.04 and 203.79 cm^{-1}, respectively, can be observed.

An atomic force microscope (Bruker Multimode 8) was used to measure the thickness of the SnS_2 nanosheets. As shown in Fig. 4(a), three areas were used to analyze the altitude intercept between the substrate and the surfaces of the SnS_2 nanosheets. According to Fig. 4(b), the heights of these three areas are 9, 8.5, and 11 nm, respectively. Based on a predicted monolayer thickness of ≈0.6 nm [35], the layer number of the SnS_2 nanosheets is about 14–18 in our experiment.

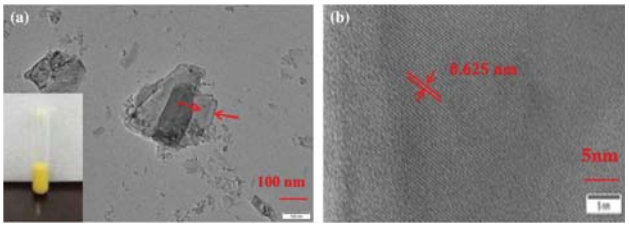

Fig. 2. (a) TEM image of the SnS_2 nanosheets. (b) The HTEM image of the SnS_2 nanosheets. Inset of (a): The SnS_2 dispersion solution.

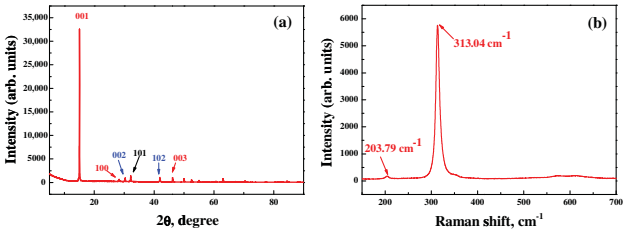

Fig. 3. (a) XRD of the SnS_2 nanosheets. (b) Raman spectrum of the SnS_2 nanosheets.

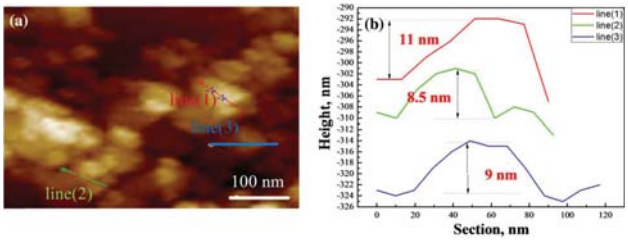

Fig. 4. (a) AFM image of the SnS_2 nanosheets. (b) The height measurement of the selected area in (a).

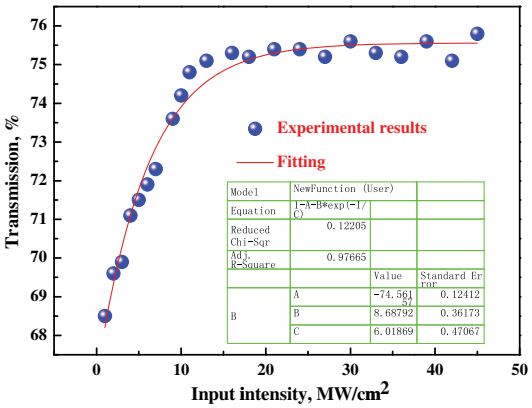

Fig. 5. Nonlinear absorption property of the SnS_2-PVA film.

Subsequently, a power-dependent transmission technique was adopted to investigate the nonlinear absorption properties of the SnS_2-PVA film-type SA [36]. The experimental results are shown in Fig. 5 and based on the following equation [15]:

$$T(I) = 1 - T_{ns} - \Delta T \times \exp(-I/I_{sat}), \quad (1)$$

where T denotes transmission, T_{ns} is non-saturable absorbance, ΔT is modulation depth, I is input intensity of laser, and I_{sat} is saturation intensity. The intensity and modulation depth have been obtained by fitting the experimental results, and are 6.01 MW/cm^2 and 8.68%, respectively.

3. EXPERIMENTAL DETAILS

Figure 6 illustrates the experimental setup of the SnS_2-PVA-based noise-like mode-locked Yb-doped fiber laser. It exhibits a linear cavity configuration made of pure normal dispersion fibers. A 980 nm laser diode (LD) with a maximum output power of 680 mW served as a pump source. The pump energy was transmitted into the cavity via a 980/1064 wave division multiplexer (WDM). A piece of 0.25 m long Yb-doped fiber (LIEKKI Yb1200-4/125) with group velocity dispersion (GVD) of 24.22 ps^2/km served as the laser gain medium. A fiber Bragg grating (FBG) with a reflectivity of 99.9% was used to prevent the light from scattering to outside the cavity. The total cavity length was 195.32 m. The GVD of the piece of 195.07 m long SMF-28 was 17.7 ps^2/km. The net dispersion of the laser cavity was estimated about ~3.46 ps^2. A polarization controller (PC) was used to adjust the polarization state in the cavity. Another FBG with a reflectivity of 60% was used to reflect light and the output laser. The output performance of the fiber laser was recorded by a fast photodetector (3G), a digital oscilloscope (DPO4054), a powermeter (PM100DS122C), an optical spectrum analyzer (AQ6317), and a spectrum analyzer (R&S FPC1000).

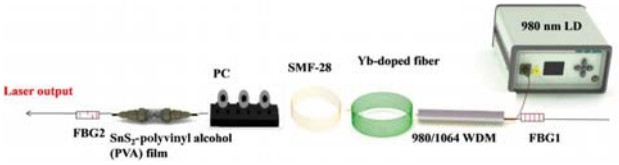

Fig. 6. Experimental setup of the noise-like mode-locked fiber laser.

4. EXPERIMENTAL RESULTS

In this experiment, the stable pulse trains were first recorded when the pump power attained 57 mW. In addition, the emission spectrum was recorded by an optical spectrum analyzer (AQ-6317) with a resolution of 0.01 nm, as shown in Fig. 7(a). The central wavelength and the 3 dB spectrum bandwidth were 1065.24 and 0.022 nm, respectively. Because reflection bandwidth of the FBG was only 0.3 nm, the corresponding 3 dB spectrum bandwidth was 0.022 nm. Figure 7(b) clearly shows the linear relationship between the pump power and the output power. The maximum output power was 9.50 mW at pump power of 422 mW, corresponding to an optical conversion efficiency of 2.25%. The calculated highest single pulse energy was 18.1 nJ. Compared with other research, high-energy noise-like mode-locking operation was first achieved using the SnS_2 nanosheets as SAs in a linear cavity. In addition, the operating photon energy of our work is 1.2 eV, which is lower than the bandgap of SnS_2 (2.24 eV), suggesting that sub-bandgap absorption is

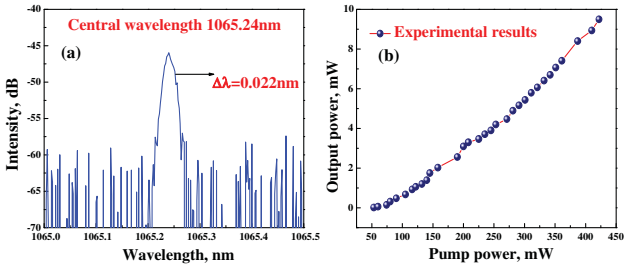

Fig. 7. (a) Emission spectrum. (b) The relationships between the average output power and pump power.

responsible for the noise-like mode-locked operation. In fact, sub-bandgap absorption phenomena have been widely reported [36–38]. It is known that there is no sub-bandgap absorption in a perfect crystal. However, in a finite system, sub-bandgap absorption at low photon energies can also be achieved, attributed to energy levels within the bandgap arising from the edge state. Thus, sub-bandgap absorption observed here was also attributed to the edge-state absorption of the SnS_2.

Figure 8 shows the typical noise-like mode-locked pulse trains and their corresponding single pulse profiles under different pump powers of 60, 190, and 422 mW. Figures 8(a)–8(c) show the typical noise-like mode-locked pulse train, and the pulse repetition rate was 526 kHz. Figures 8(d)–8(f) show the single pulse profile; the pulse width increased from 0.18 to 0.36 μs when the pump power rose from 60 to 422 mW. In this experiment, since the value of the reflection bandwidth in the linear cavity was only 0.3 nm, we obtained a noise-like mode-locked pulse train rather than a passively mode-locked pulse train. In addition, the wide single pulse width was attributed to the large value of dispersion (~3.46 ps^2) and the long length of the cavity (~195.32 m).

To characterize the stability of the noise-like mode-locked fiber laser, a spectrum analyzer (R&S FPC1000) was employed to record the radio frequency (RF) spectrum. Figure 9(a) shows the RF spectrum located at a fundamental repetition rate of 526 kHz with a resolution of 300 Hz. The signal-to-noise ratio was nearly 44 dB. Figure 9(b) shows the RF spectrum within a wide bandwidth of 8 MHz. All the results verify that noise-like mode-locked pulses with a high stability were obtained.

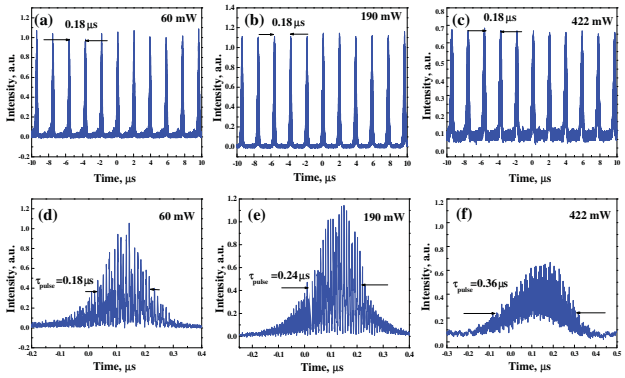

Fig. 8. Typical oscilloscope traces and single pulse profiles of the noise-like mode-locked pulse trains under different pump powers: (a), (d) 60 mW; (b), (e) 190 mW; (c), (f) 422 mW.

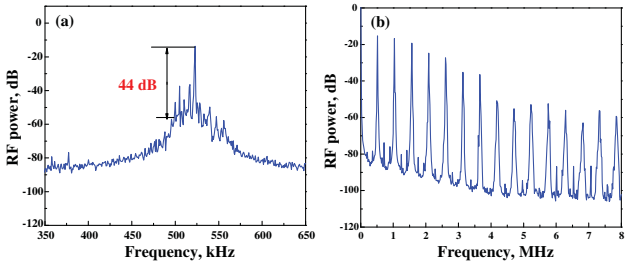

Fig. 9. (a) RF spectrum of the noise-like mode-locked laser located at 526 kHz. (b) RF spectrum with a bandwidth of 8 MHz.

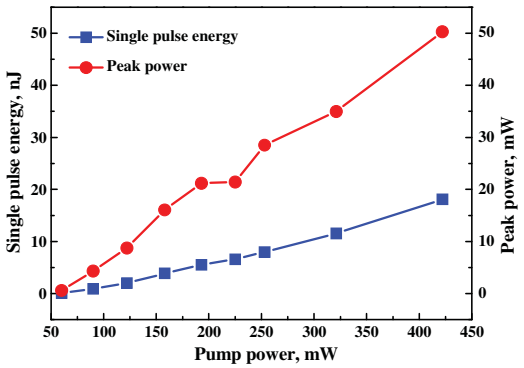

Fig. 10. Single pulse energy and the peak power as a function of the pump power.

As shown in Fig. 10, when the pump power rose from 60 to 422 mW, the single pulse energy increased from 0.104 to 18.1 nJ. The peak power was up-regulated 0.58–50.28 mW.

However, some aspects in our experiment need further improvement, e.g., the method of preparation of the SA can be replaced using a chemical vapor deposition (CVD) method; the length of cavity may become shorter than before; the reflection bandwidth of the FBG can be larger.

5. CONCLUSION

We have first achieved high-energy noise-like mode-locking operation using SnS_2 nanosheets as SAs in a linear cavity. The maximum output power and the highest single pulse energy under a pump power of 422 mW were 9.50 mW and 18.1 nJ, respectively. The saturation intensity and modulation depth were about 6.01 MW/cm^2 and 8.68%, respectively. When the pump power rose from 60 to 422 mW, the pulse width increased from 0.18 to 0.36 μs with a pulse repetition rate of 526 kHz. Our experimental results verify that SnS_2-PVA film exhibits excellent performance in obtaining high-energy noise-like mode-locking operation.

Funding. Natural Science Foundation of Shandong Province (2017GGX20120, ZR2016FP01); China Postdoctoral Science Foundation (2016M602177); National Natural Science Foundation of China (NSFC) (11674199, 11804196, 61205174).

REFERENCES

1. N. Ming, S. N. Tao, W. Q. Yang, Q. Y. Chen, R. Y. Sun, C. Wang, S. Y. Wang, B. Y. Man, and H. N. Zhang, "Mode-locked Er-doped fiber laser based on PbS/CdS core/shell quantum dots as saturable absorber," Opt. Express **26**, 9017–9026 (2018).
2. S. Sathiyan, V. Velmurugan, K. Senthilnathan, P. R. Babu, and S. Sivabalan, "All-normal dispersion passively mode-locked Yb-doped fiber laser using MoS_2–PVA saturable absorber," Laser Phys. **26**, 055103 (2016).
3. Q. X. Guo, H. P. Si, Z. Y. Lu, X. L. Han, B. Y. Man, D. J. Feng, H. N. Zhang, and S. Z. Jiang, "Passively mode-locked dual-wavelength Er-doped fiber laser based on antimony tin oxide as saturable absorber," Laser Phys. **29**, 045801 (2019).

4. L. N. Duan, X. M. Liu, D. Mao, L. R. Wang, and G. X. Wang, "Experimental observation of dissipative soliton resonance in an anomalous-dispersion fiber laser," Opt. Express **20**, 265–270 (2012).
5. A. F. J. Runge, C. Aguergaray, N. G. R. Broderick, and M. Erkintalo, "Coherence and shot-to-shot spectral fluctuations in noise-like ultrafast fiber lasers," Opt. Lett. **38**, 4327–4330 (2013).
6. J. Liu, Y. Chen, P. H. Tang, C. W. Xu, C. J. Zhao, H. Zhang, and S. C. Wen, "Generation and evolution of mode-locked noise-like square-wave pulses in a large-anomalous-dispersion Er-doped ring fiber laser," Opt. Express **23**, 6418–6427 (2015).
7. D. Y. Tang, L. M. Zhao, and B. Zhao, "Soliton collapse and bunched noise-like pulse generation in a passively mode-locked fiber ring laser," Opt. Express **13**, 2289–2294 (2005).
8. B. Guo, "2D noncarbon materials-based nonlinear optical devices for ultrafast photonics," Chin. Opt. Lett. **16**, 020004 (2018).
9. G. Steinmeyer, D. H. Sutter, L. Gallmann, N. Matuschek, and U. Keller, "Frontiers in ultrashort pulse generation: pushing the limits in linear and nonlinear optics," Science **286**, 1507–1512 (1999).
10. U. Keller, "Recent developments in compact ultrafast lasers," Nature **424**, 831–838 (2003).
11. O. Okhotnikov, A. Grudinin, and M. Pessa, "Ultra-fast fibre laser systems based on SESAM technology: new horizons and applications," New J. Phys. **6**, 177 (2004).
12. D. P. Zhou, L. Wei, B. Dong, and W. K. Liu, "Tunable passively Q-switched erbium-doped fiber laser with carbon nanotubes as a saturable absorber," IEEE Photon. Technol. Lett. **22**, 9–11 (2010).
13. H. Zhang, Q. L. Bao, D. Y. Tang, L. M. Zhao, and K. P. Loh, "Large energy soliton erbium-doped fiber laser with a graphene-polymer composite mode locker," Appl. Phys. Lett. **95**, 141103 (2009).
14. N. N. Xu, N. Ming, X. L. Han, B. Y. Man, and H. N. Zhang, "Large-energy passively Q-switched Er-doped fiber laser based on CVD-Bi_2Se_3 as saturable absorber," Opt. Mater. Express **9**, 373–383 (2019).
15. B. H. Chen, X. Y. Zhang, K. Wu, H. Wang, J. Wang, and J. P. Chen, "Q-switched fiber laser based on transition metal dichalcogenides MoS_2, $MoSe_2$, WS_2, and WSe_2," Opt. Express **23**, 26723–26737 (2015).
16. D. Mao, X. Y. She, B. B. Du, D. X. Yang, W. D. Zhang, K. Song, X. Q. Cui, B. Q. Jiang, T. Peng, and J. L. Zhao, "Erbium-doped fiber laser passively mode locked with few-layer WSe_2/$MoSe_2$ nanosheets," Sci. Rep. **6**, 23583 (2016).
17. J. Du, Q. K. Wang, G. B. Jiang, C. W. Xu, C. J. Zhao, Y. J. Xiang, Y. Chen, S. C. Wen, and H. Zhang, "Ytterbium-doped fiber laser passively mode locked by few-layer molybdenum disulfide (MoS_2) saturable absorber functioned with evanescent field interaction," Sci. Rep. **4**, 6346–6352 (2014).
18. D. Mao, Y. D. Wang, C. J. Ma, L. Han, B. Q. Jiang, X. T. Gan, S. J. Hua, W. D. Zhang, T. Mei, and J. L. Zhao, "WS_2 mode-locked ultrafast fiber laser," Sci. Rep. **5**, 7965–7971 (2015).
19. P. G. Yan, A. J. Liu, Y. S. Chen, J. Z. Wang, S. C. Ruan, H. Chen, and J. F. Ding, "Passively mode-locked fiber laser by a cell-type WS_2 nanosheets saturable absorber," Sci. Rep. **5**, 12587–12593 (2015).
20. Z. Q. Luo, Y. Z. Huang, M. Zhong, Y. Y. Li, J. Y. Wu, B. Xu, H. Y. Xu, Z. P. Cai, J. Peng, and J. Weng, "1, 1.5, and 2 μm fiber lasers Q-switched by a broadband few-layer MoS_2 saturable absorber," J. Lightwave Technol. **32**, 4679–4686 (2014).
21. R. I. Woodward, R. C. T. Howe, T. H. Runcorn, G. Hu, F. Torrisi, E. J. R. Kelleher, and T. Hasan, "Wideband saturable absorption in few-layer molybdenum diselenide ($MoSe_2$) for Q-switching Yb-, Er- and Tm-doped fiber lasers," Opt. Express **23**, 20051–20061 (2015).
22. M. S. Yang, J. Yu, S. Z. Jiang, C. Zhang, Q. Q. Sun, M. H. Wang, H. Zhou, C. H. Li, B. Y. Man, and F. C. Lei, "High stability luminophores: fluorescent $CsPbX_3$ (X = Cl, Br and I) nanofiber prepared by one-step electrospinning method," Opt. Express **26**, 20649–20660 (2018).
23. K. Wu, X. Y. Zhang, J. Wang, X. Li, and J. P. Chen, "WS_2 as a saturable absorber for ultrafast photonic applications of mode-locked and Q-switched lasers," Opt. Express **23**, 11453–11461 (2015).
24. R. Y. Sun, H. N. Zhang, and N. N. Xu, "High-power passively Q-switched Yb-doped fiber laser based on tin selenide as a saturable absorber," Laser Phys. **28**, 085105 (2018).
25. K. D. Niu, Q. Y. Chen, R. Y. Sun, B. Y. Man, and H. N. Zhang, "Passively Q-switched erbium-doped fiber laser based on SnS_2 saturable absorber," Opt. Mater. Express **7**, 3934–3943 (2017).
26. Y. D. Cui, F. F. Lu, and X. M. Liu, "Nonlinear saturable and polarization-induced absorption of rhenium disulfide," Sci. Rep. **7**, 40080 (2017).
27. F. F. Lu, "Passively harmonic mode-locked fiber laser based on ReS_2 saturable absorber," Mod. Phys. Lett. B **31**, 1750206 (2017).
28. J. W. Seo, J. T. Jang, S. W. Park, C. J. Kim, B. W. Park, and J. W. Cheon, "Two-dimensional SnS_2 nanoplates with extraordinary high discharge capacity for lithium ion batteries," Adv. Mater. **20**, 4269–4273 (2008).
29. B. Luo, Y. Fang, B. Wang, J. Zhou, H. H. Song, and L. J. Zhi, "Two dimensional graphene-SnS_2 hybrids with superior rate capability for lithium ion storage," Energy Environ. Sci. **5**, 5226–5230 (2012).
30. J. T. Kai, K. X. Wang, Y. Z. Su, X. F. Qian, and J. S. Chen, "High stability and superior rate capability of three-dimensional hierarchical SnS_2 microspheres as anode material in lithium ion batteries," J. Power Sources **196**, 3650–3654 (2011).
31. A. J. Smith, P. E. Meek, and W. Y. Liang, "Raman scattering studies of SnS_2 and $SnSe_2$," J. Phys. C **10**, 1321–1323 (1977).
32. K. D. Niu, R. Y. Sun, Q. Y. Chen, B. Y. Man, and H. N. Zhang, "Passively mode-locked Er-doped fiber laser based on SnS_2 nanosheets as a saturable absorber," Photon. Res. **6**, 72–76 (2018).
33. H. Zhang, D. Y. Tang, L. M. Zhao, Q. L. Bao, and K. P. Loh, "Large energy mode locking of an erbium-doped fiber laser with atomic layer graphene," Opt. Express **17**, 17630–17635 (2009).
34. L. Li, Y. G. Wang, X. Wang, T. Lin, and H. Sun, "High energy mode-locked Yb-doped fiber laser with Bi_2Te_3 deposited on tapered-fiber," Optik **142**, 470–474 (2017).
35. J. H. Ahn, M. J. Lee, H. Heo, J. H. Sung, K. Kim, H. Hwang, and M. H. Jo, "Deterministic two-dimensional polymorphism growth of hexagonal n-type SnS_2 and orthorhombic p-type SnS crystals," Nano Lett. **15**, 3703–3708 (2015).
36. B. Guo, Q. Lyu, Y. Yao, and P. F. Wang, "Direct generation of dip-type sidebands from WS_2 mode-locked fiber laser," Opt. Mater. Express **6**, 2475–2486 (2016).
37. R. I. Woodward, E. J. R. Kelleher, R. C. T. Howe, G. Hu, F. Torrisi, T. Hasan, S. V. Popov, and J. R. Taylor, "Tunable Q-switched fiber laser based on saturable edge-state absorption in few-layer molybdenum disulfide (MoS_2)," Opt. Express **22**, 31113–31122 (2014).
38. S. X. Wang, H. H. Yu, H. J. Zhang, A. Z. Wang, M. W. Zhao, Y. X. Chen, L. M. Mei, and J. Y. Wang, "Broadband few-layer MoS_2 saturable absorbers," Adv. Mater. **26**, 3538–3544 (2014).

120.192.27.116 {ts '2019-07-25 00:12:02'}